A Low Frequency OTA Design with Temperature-Insensitive Variable Transconductance Using 180-nm CMOS Technology

Nanang Sulistiyanto, *Student Member*, IEEE,
Chua-Chin Wang, *Senior Member*, IEEE
Department of Electrical Engineering
National Sun Yat-Sen University
Kaohsiung, Taiwan 80424
e-mail: ccwang@ee.nsysu.edu.tw

Robert Rieger, *Senior Member*, IEEE
Institute of EEIT
Keil University
Keil, Germany
e-mail: rri@tf.uni-kiel.de

***Abstract*— This paper presents a low-frequency OTA featured with a feedback loop stabilized by an OTA to auto-adjust bias currents of other OTAs. By using a symmetrical OTA with a degenerated MOS resistor, the proposed design results in less than 1% gain variation for the frequency band <5 kHz. The proposed OTA relaxes the design difficulty for biosensing in low frequency range to make amplification and low-pass filtering feasible.**

Keywords-temperature variation; biopotential preprocessing; negative feedback; variable gain amplifier; OTA

I. INTRODUCTION

Digital signal processing systems (DSPs) play a very important role in the recent technology trend because of the robustness and flexibility, especially for Medicare instruments which mainly depend on measurement of biopotential signals such as ECG, EEG, and EMG (i.e., ExG). Although high performance digital systems have been successfully developed and implemented, analog preamplifiers and antialiasing filters may limit the expected high performance of those DSPs, because the sampled and converted digital signals might lose the fidelity due to the poor functionality of their corresponding preprocessing stage. As a solution, digitally assisted analog amplifiers [1−3] and filters [4−6] have been introduced to extend capability of digital systems in controlling amplitude, bandwidth, as well as quality of input signals. The digital control mechanism by the DSPs could be very useful to realize a general purpose single chip solution which is adequate to process ExG signals or other sensor interfaces [7−8] and generate reliable outcome.

High gain opamps (OPAs) have been successfully implemented as basic building blocks of amplifiers and RC filters. Using conventional negative feedback designs with very high gain OPAs, the systems are robust to PVT (process, voltages, temperature) variations. However, an OPAs commonly consume, which is disadvantages for portable applications. As an alternative, gm-C designs [4−6, 9−11] can provide low power and tunable filters. However, these designs are sensitive to PVT variations.

Recently, negative feedback designs of amplifier replicas were reported to resist PVT variations. Firstly, an LPF replica was reported to design a MOSFET C BPF for biomedical applications [12]. A reference pulse signal to control voltage bias of the MOSFETs to get a constant cutoff frequency. Secondly, a push-pull opamp replica was implemented to attain a consistent bandwidth [13]. The system uses an opamp-based negative feedback to bias the push-pull opamps adaptively. Thirdly, a replica of a near sub-threshold operated LNA was demonstrated to generate a consistent gain by comparing to a constant current source [14].

In this paper, we propose a feedback design for low frequency OTAs to attain a linear variable gain by using simple current dividers and multipliers. To verify the performance, 180 nm CMOS technology is used to carry out the entire design with all PVT-corner simulations.

II. OTA AND FEEDBACK SYSTEM

A. OTA Circuit Design

Fig. 1 shows the proposed two-stage OTA circuit with a degenerated MOS resistor R_{dg} composed of biased transistors, M107 to M128. Without R_{dg}, transconductance g_{m1} is derivate as Eqn. (1), where K_p is PMOS transconductance parameter, I_b is the tail current, W_{129} and

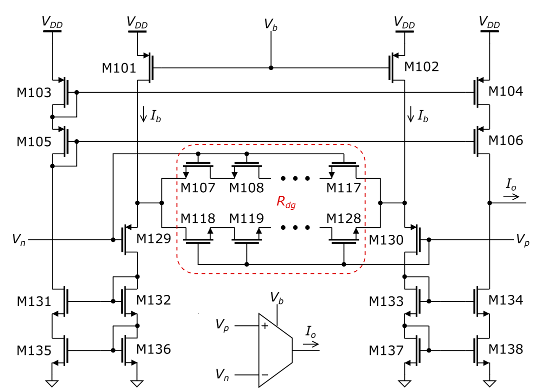

Figure 1. Proposed symmetrical two-stage OTA circuit

L_{129} are wide and length of MOS129, respectively. Therefore, total transconductance g_m is derived in Eqn. (2). High R_{dg} will result in a relatively wide input range (–50 to 50 mV) as shown in Fig. 2.

$$g_{m1} = (0.5K_pI_bW_{129}/L_{129})^{0.5} \quad (1)$$

$$g_m = g_{m1}/(2+g_{m1}R_{dg}) \quad (2)$$

Fig. 3 shows frequency responses of the OTA with various tail currents. Phases of the OTA indicates that the OTA is stable for frequency <10 kHz, which is the range of ExG signals. The tail current is limited to 80 nA because the output current of the OTA does not monotonically increase for the current >80 nA as shown in Fig. 4.

B. *Feedback System for Stabilization*

Fig. 5 shows the proposed feedback system for constant g_m over temperature range of –50 to 150°C. N_1 and N_2 are scaling factors of current divider and amplifier, respectively. N_3 is a scaling factor of the second current mirror (M205 to M224) that produces I_b. Finally, A_{bo} is an approximation gradient value estimated from Fig. 4. Reference OTA is operated close to the mid voltage of V_m with a small constant differential voltage aV_m (the voltage division by R_{m1} and R_{m2}). Therefore, its output current I_o is proportional to its g_m.

I_r is a setting current (generated by a current output DAC attenuated by N_1) to control g_m linearly. The first current mirror (M201 to M204) subtracts I_o from I_r. A high open loop gain G in Eqn. (3) will steer I_o close to I_r. Fig. 6 shows a simplified diagram of the feedback system. Its transfer function is given in Eqn. (4). R_b is the input impedance of the second current mirror, and C_b is an external compensation capacitor (10 nF). If $I_r(t)$ is a unit step $u(t)$, $I_o(t)$ can be attained as Eqn. (5). Because G is much higher than the unit gain, the steady state of $I_o(t)$ will approach $I_r(t)$.

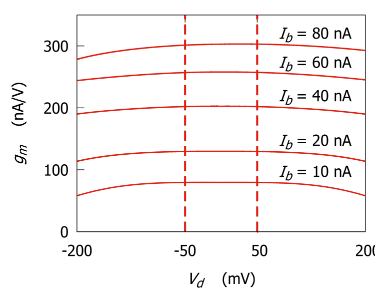

Figure 2. Input range of designed OTA (−50 to 50 mV)

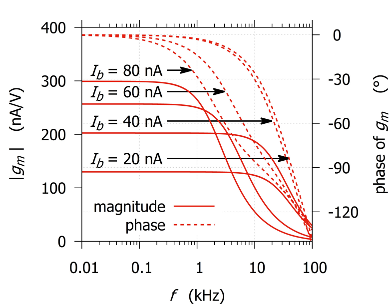

Figure 3. Frequency responses of the OTA with various tail currents

$$G = N_2N_3A_{bo} \quad (3)$$

$$I_o/I_r = G/(1+G+sR_bC_b) \quad (4)$$

$$I_o(t) = G\cdot u(t)/(1+G) + \exp(-t(1+G)/(R_bC_b)) \quad (5)$$

When temperature changes, the system auto-adjusts I_b to keep I_o stable. The system also adjusts tail currents of controlled OTAs via bias voltage V_b. Because of the same bias circuits as in reference OTA (M201), the OTAs will be activated with the same tail currents to generate the same transconductances.

Mismatch on the first current mirror will result in deviation (or offset) ΔI_o so that $\Delta I_b \approx \Delta I_o/A_{ob} \approx 16\Delta I_o$ and then $\Delta g_m \approx (\Delta I_b)^{0.5} \approx 4(\Delta I_b)^{0.5}$. This indicates that the current mirror have to be design carefully so that $\Delta I_o/I_o < 0.1\%$. On the other hand, the other current mirrors will result in deviation ΔG. If $(G+\Delta G)$ is much higher than the unit gain, the deviation can be neglected. Notably, C_b suppress random noise contaminating I_o, which can spread into all OTAs via V_b.

C. *Current Divider Design*

Current dividers in Fig. 5 are classified into 2 types: unbiased and biased current dividers as shown in Fig. 7 and 8, respectively. An NMOS current mirror circuit (M323 to M334) divides I_r by 10 and then another PMOS current mirror circuit (M301 to M322) further divides the previous outcome by 10. Thus, the I_r/100 is generated. Fig. 8 shows a

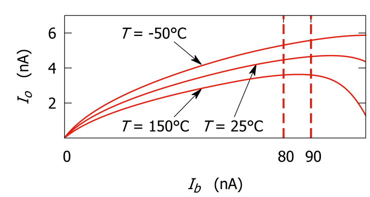

Figure 4. Nonlinear characteristic of output current I_o

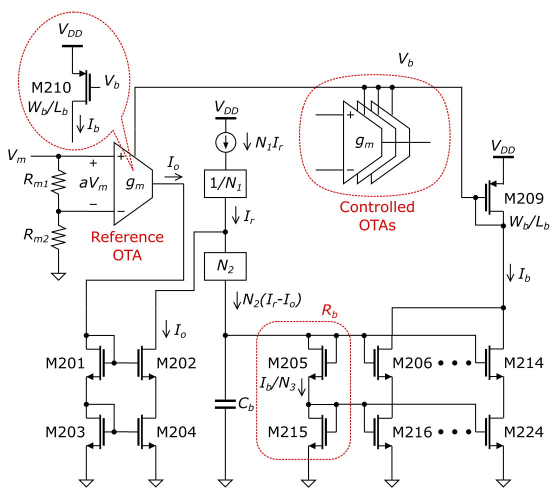

Figure 5. Proposed feedback system

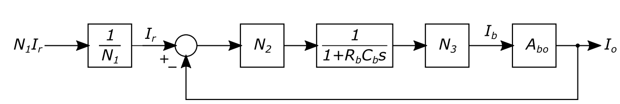

Figure 6. Simplified diagram block of the proposed feedback system

biased current mirror circuit (M401 to M416) performing division by 3. Cascading one unbiased divider and two biased dividers result in N_1 = 900. Notably, a bias circuit (M417 to M426) provides all bias voltages.

D. Current Multiplier Design

Fig. 9 shows the current multiplier design in Fig. 5, which is basically a current mirror circuit (M501 to M516) to multiply input current by 3. The previous bias circuit provides required bias voltages. Cascading 6 of the biased current amplifiers will result in $N_2 = 729$.

III. Simulation and Comparison

All of mentioned circuits are realized using 0.18 µm CMOS process. We firstly investigate the performance of the feedback system and then a controlled OTA in a simple gm-C low pass filter, as shown in Fig. 10.

A. Verification of Feedback System

To verify the system stability, an input pulse current (I_r) is applied to the system input such that I_b becomes higher than 80 nA as shown in Fig. 11. Considering that I_o tends to converge to I_r, this indicates that the system is still stable even I_b reaches 90 nA. This agrees with the curve at 25°C in Fig. 4, where it monotonically increases until I_b = 90 nA.

I_o varies nearly exponentially as predicted in Eqn. (5). However, the rising time (about 30 ms) is nearly three times than the falling time (about 10 ms). This is because R_b is changed greatly by I_b. Low I_b result in high R_b or a long time constant, which results in slow rising of I_b. By contrast, high I_b results in a short time constant, and consequently, a fast falling time of I_b.

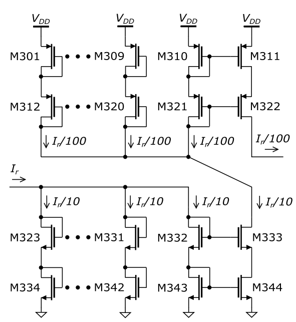

Figure 7. Unbiased current divider circuit (÷100)

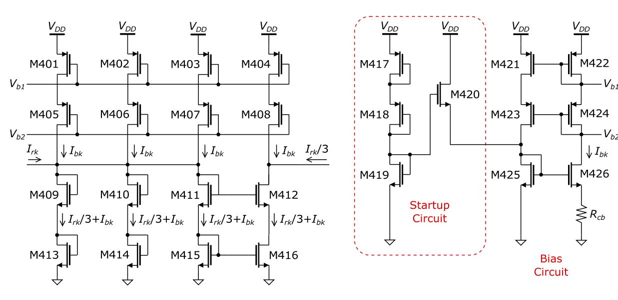

Figure 8. Biased current divider circuit (÷3)

B. Application to Low Pass Filter

Fig. 12 shows frequency responses of the low pass filter using a controlled OTA at two extreme conditions. The worst gain decreasing at frequencies lower than 5 kHz is also 1%. Fig. 13 shows linear bandwidth adjustment of the filter using I_r because of gm-C design.

Performance comparison with recent filters is summarized in Table I. Figure of Merit (FOM) is determined based on Eqn. (6), where B is bandwidth, ΔT is temperature range, σ is deviation, P is consumed power, and V_{DD} is supply voltage. The previous work [15] did not claim to use controlled OTAs so that the proposed OTAs are assumed to be implemented in the work. According to normalized FOM tabulated in Table I, this work is significantly better than the previous works [12] and [15] because of wider bandwidth and much lower power consumption. On the other hand, although [14] has a very high FOM score because of its wide bandwidth, it is not in the range of biosignal bandwidth. In conclusion, the proposed design demonstrates the best deviation and the widest temperature range for bio medical signal processing.

$$FOM = B \cdot \Delta T / (\sigma \cdot P \cdot V_{DD}) \quad (6)$$

IV. Conclusion

Detailed simulation results show that the proposed feedback system work properly as expected to result in OTAs with controllable and consistent transconductances at frequencies <5 kHz which is adequate for biosignal

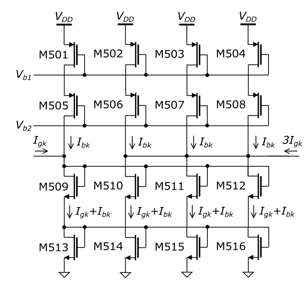

Figure 9. Biased current multiplier circuit (×3)

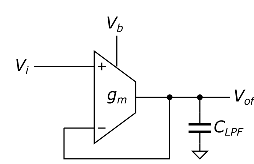

Figure 10. Low pass filter circuits

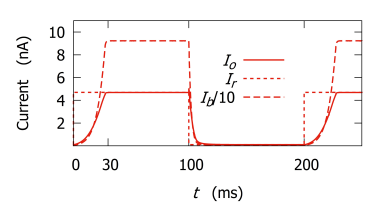

Figure 11. Transient responses of the proposed feedback system

processing. The worse settling time of 30 ms is fast enough to cope with temperature changes in human body environment. Low pass filtering result in good performances over temperature range of –50 to 150°C. This indicates that the proposed analog systems might be embedded with a high performance DSP to carry out very accurate biosensing.

TABLE I. TABLE TYPE STYLES

	[12]	[15]	[14]	**This work**
Year	2010	2014	2015	**2019**
Process (nm)	130	65	65	**180**
V_{DD} (V)	1.2	2.5	0.6	**3**
Bandwidth	30 Hz	5 kHz[a]	2.14 GHz	**5 kHz**
Deviation	1%	0.22%	8.3%	**1%**
Power	200 nW	5 mW	402 µW	**7 µW**
Normalized FOM	0.263	0.007	2918	**1**

a. Based on an assumption

ACKNOWLEDGMENT

This research was partially supported by Minister of Science and Technology under grant MOST 107-2218-E-110-016-, and 107-2218-E-110-004-. The authors would like to express their deepest gratefulness to TSRI (Taiwan Semiconductor Research Institute, which was called CIC before) of NARL (National Applied Research Laboratories), Taiwan, for the EDA support service.

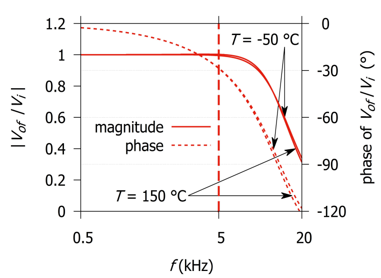

Figure 12. Frequency response of the filter at two extreme temperatures

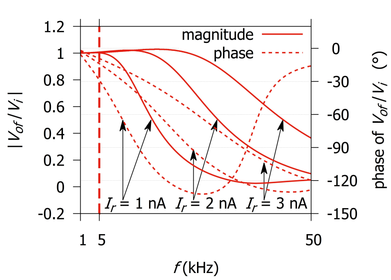

Figure 13. Linear adjustment of filter gain by input current I_r

REFERENCES

[1] A. Bagheri, M. T. Salam, J. L. P. Velazquez and R. Genov, "Low-frequency noise and offset rejection in DC-coupled neural amplifiers: a review and digitally-assisted design tutorial," *IEEE Trans. Biomed. Circuits Syst.*, vol. 11, no. 1, pp. 161-176, Feb. 2017, doi: 10.1109/TBCAS.2016.2539518.

[2] H. Bhamra, J. Lynch, M. Ward and P. Irazoqui, "A noise-power-area optimized biosensing front end for wireless body sensor nodes and medical implantable devices," *IEEE Trans. Very Large Scale Integr. (VLSI) Syst.*, vol. 25, no. 10, pp. 2917-2928, Oct. 2017, doi: 10.1109/TVLSI.2017.2714171.

[3] R. Rieger and N. Sulistiyanto, "Integrated circuit for super-regenerative low-frequency amplification," *IEEE Trans. Circuits Syst. II, Exp. Briefs*, vol. 65, no. 1, pp. 31-35, Jan. 2018, doi: 10.1109/TCSII.2017.2672782.

[4] R. Gangarajaiah, M. Abdulaziz, H. Sjöland, P. Nilsson and L. Liu, "A digitally assisted nonlinearity mitigation system for tunable channel select filters," *IEEE Trans. Circuits Syst. II, Exp. Briefs*, vol. 63, no. 1, pp. 69-73, Jan. 2016, doi: 10.1109/TCSII.2015.2504272.

[5] L. B. Leene and T. G. Constandinou, "Time domain processing techniques using ring oscillator-based filter structures," *IEEE Trans. Circuits Syst. I, Reg. Papers*, vol. 64, no. 12, pp. 3003-3012, Dec. 2017, doi: 10.1109/TCSI.2017.2715885.

[6] M. B. Elamien and S. A. Mahmoud, "An 114 Hz–12 MHz digitally controlled low-pass filter for biomedical and wireless applications," *IET Circ. Device Syst.*, vol. 12, no. 5, pp. 606-614, Sept. 2018, doi: 10.1049/iet-cds.2017.0410.

[7] A. Depari et al., "Autobalancing analog front end for full-range differential capacitive sensing," *IEEE Trans. Instrum. Meas.*, vol. 67, no. 4, pp. 885-893, April 2018, doi: 10.1109/TIM.2017.2785160

[8] G. Barile et al., "A CMOS full-range linear integrated interface for differential capacitive sensor readout," *Sens. Actuators A Phys.*, vol. 281, pp. 130-140, 2018, doi: 10.1016/j.sna.2018.08.033.

[9] C. Sawigun and S. Thanapitak, "A 0.9-nW, 101-Hz, and 46.3-µVrms IRN low-pass filter for ECG acquisition using FVF biquads," *IEEE Trans. Very Large Scale Integr. (VLSI) Syst.*, vol. 26, no. 11, pp. 2290-2298, Nov. 2018, doi: 10.1109/TVLSI.2018.2863706.

[10] S. Thanapitak and C. Sawigun, "A subthreshold buffer-based biquadratic cell and its application to biopotential filter design," IEEE Trans. Circuits Syst. I, Reg. Papers, vol. 65, no. 9, pp. 2774-2783, Sept. 2018, doi: 10.1109/TCSI.2018.2808361.

[11] C. Sawigun and S. Thanapitak, "A nanopower biopotential lowpass filter using subthreshold current-reuse biquads with bulk effect self-neutralization," *IEEE Trans. Circuits Syst. I, Reg. Papers*, to be published. doi: 10.1109/TCSI.2018.2885954.

[12] K. Choo, W. Lee and S. Cho, "A PVT tolerant BPF using turn-off MOSFET for bio applications in 0.13µm CMOS," in *Proc. 7th Int. SoC Design Conf. (ISOCC 2010)*, Incheon, Korea, Nov. 22-23, 2010, pp. 420-423, doi: 10.1109/SOCDC.2010.5682882.

[13] L. Ye, C. Shi, H. Liao, R. Huang and Y. Wang, "Highly power-efficient active-RC filters with wide bandwidth-range using low-gain push-pull opamps," *IEEE Trans. Circuits Syst. I, Reg. Papers*, vol. 60, no. 1, pp. 95-107, Jan. 2013, doi: 10.1109/TCSI.2012.2215700.

[14] V. M. M., R. Paily and A. Mahanta, "A new PVT compensation technique based on current comparison for low-voltage, near sub-threshold LNA," *IEEE Trans. Circuits Syst. I, Reg. Papers*, vol. 62, no. 12, pp. 2908-2919, Dec. 2015, doi: 10.1109/TCSI.2015.2486078.

[15] C. Chu and Y. Wang, "A PVT-independent constant-gm bias technique based on analog computation," *IEEE Trans. Circuits Syst. II, Exp. Briefs*, vol. 61, no. 10, pp. 768-772, Oct. 2014, doi: 10.1109/TCSII.2014.2345296.